EMI Reduction in an Interleaved Buck Converter Through Spread Spectrum Frequency Modulation

EMI Reduction in an Interleaved Buck Converter Through Spread Spectrum Frequency Modulation

Emmanuel Stok
Eindhoven University of Technology, NL
e.p.stok@tue.nl

Marald Otten
Lightyear, NL
marald.otten@lightyear.one

Henk Huisman
Eindhoven University of Technology, NL
H.Huisman.stok@tue.nl

Yusuf Kösesoy
Eindhoven University of Technology, NL
y.k.kosesoy@tue.nl

ACKNOWLEDGMENT

This project has received funding from the ECSEL Joint Undertaking (JU) under grant agreement No 101007281. The JU receives support from the European Union's Horizon 2020 research and innovation programme and Austria, Germany, Slovenia, Netherlands, Belgium, Slovakia, France, Italy, Turkey.

***Index Terms*—EMC/EMI, Modulation Scheme, Gallium-Nitride (GaN), High-Frequency Power Converter, Interleaved Converters.**

***Abstract*—Spread spectrum frequency modulation is applied in a high-frequency DC/DC power converter to reduce conducted EMI. A new modulation biasing technique is developed to further reduce EMI levels in converters equipped with hardware filters. In the lab, this biasing shows effective shaping of the EMI spectrum.**

I. Introduction

SWITCHED mode power converters are the basis for high efficiency electrical power conversion. For solar electric vehicles this is especially important, such that they can make the most of the limited solar energy they can capture [1]. Besides maximising the efficiency of the conversion action directly, the ultimate goal is maximum efficiency of the vehicle as a whole. The size and weight of the converters impact the power usage and aerodynamic performance of the vehicle.

Much work is already done in making DC/DC converters more power dense, often by increasing switching frequency and thus reducing size requirements for passive components [2]. But increased switching frequencies push the switching harmonics higher in the frequency spectrum with typically more stringent conducted electromagnetic compatibility (EMC) limits [3]. In this case, more filtering may be required to meet any applicable EMC standards. The filters must be relatively large to dampen the harmonic peaks of the switching frequency [4] at these relatively low frequencies.

Spread spectrum frequency modulation (SSFM) is a modulation strategy which can reduce the switching harmonic EMI peaks generated by the converter and is well suited for converters with high switching frequencies [4]–[14]. Originating in the communications sector [15], SSFM purposefully spreads a signal over a larger frequency band. In power converters, this is often done by modulation with a periodic signal, known as periodic SSFM [4], [6], [11], [12].

However, only [6] explores the application of SSFM to an interleaved converter. Also, there is a lack of comprehensive information regarding the effect of the modulation on efficiency.

This paper will evaluate different variations of Periodic SSFM for application in a 2-phase interleaved buck converter utilizing GaN HEMTs (shown in Fig. 1), with the goal of reducing conducted EMI. Through simulation the periodic SSFM strategy is validated for this interleaved buck and the best modulation parameters are found. A new biased SSFM strategy is also presented for converters that also include hardware EMI filtering. Finally, these modulations are then applied on a hardware prototype where conducted EMI and efficiency are measured.

II. Periodic Spread Spectrum Frequency Modulation

A. Overview

The fundamental switching cycle of a switched mode power converter is responsible for a narrow and intense peak in the frequency spectrum, located at the switching frequency. An example is shown by the blue trace in Fig. 2. Due to the frequency composition of the square wave, this peak is followed by numerous subsequent peaks

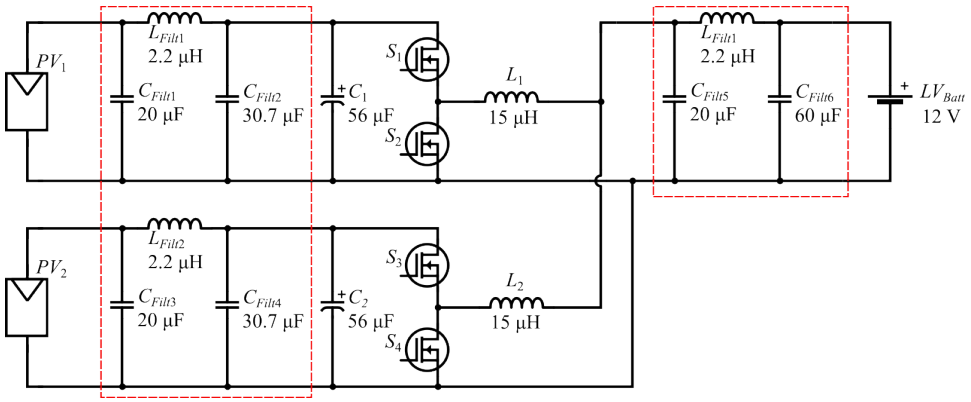

Fig. 1: Circuit schematic of the interleaved buck converter with input and output filters marked in red

located at the harmonics of the switching frequency (not shown). By modulating the frequency of this switching cycle with SSFM, these narrow peaks devolve into a broader spectrum with a lesser peak magnitude, as shown with the first harmonic in Fig. 2.

Some parameters are introduced when discussing SSFM:

- f_c, The central switching frequency of the converter
- Δf_c, The amplitude of the modulation
- f_m, The frequency of the modulation pattern

The general effect of these parameters in the frequency spectrum is shown in Fig. 2. The Δf_c is responsible for the width of the spreading, while f_m changes the distance between the multiple spread spectrum peaks.

B. Analytical Determination of the effect of SSFM

The width of the total spreading can be estimated by Carson's Bandwidth Rule (CBR) [5],

$$\text{CBR} = 2(\Delta f_c + f_m). \tag{1}$$

The resulting peak values of the SSFM are more complicated to estimate. A first estimate would be to calculate the new peak value assuming an even and flat-topped repartition of the harmonic peak signal energy into a broadband spread spectrum signal as shown in Fig. 3.

According to Parseval's theorem, the energy of the signal can be calculated via integration in frequency domain the same as in time domain. As such, the power integration of two signals in the frequency domain can be directly compared as expressed in (2):

$$\int_{f_a}^{f_b} |X_{\text{mod}}(2\pi f)|^2 \, \mathrm{d}f = \int_{f_a}^{f_b} |X_{\text{NOmod}}(2\pi f)|^2 \, \mathrm{d}f, \tag{2}$$

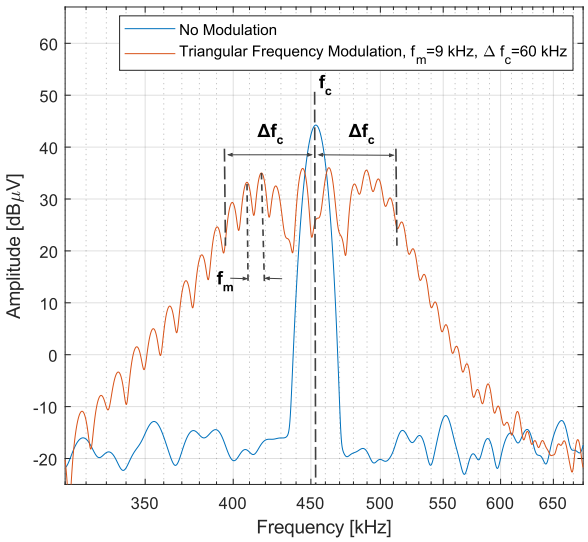

Fig. 2: The effect of basic spread spectrum modulation parameters on the average frequency spectrum measurement of the input of a buck converter, as simulated with SPICE

where X_{mod} and X_{NOmod} are the Fourier transforms of the original time domain voltage signals, and f_a and f_b are set by the CBR around the harmonic frequency of interest. In this case for the first harmonic,

$$f_a = f_c - \Delta f_c - f_m, \tag{3}$$

and,

$$f_b = f_a + \text{CBR} = f_c + \Delta f_c + f_m. \tag{4}$$

As the resulting SSFM frequency spectrum is assumed to be rectangular, (2) can be simplified to:

$$(\text{CBR})(\text{SSFM}_{\text{peak}}) = \int_{f_a}^{f_b} |X_{\text{NOmod}}(2\pi f)|^2 \, \mathrm{d}f, \tag{5}$$

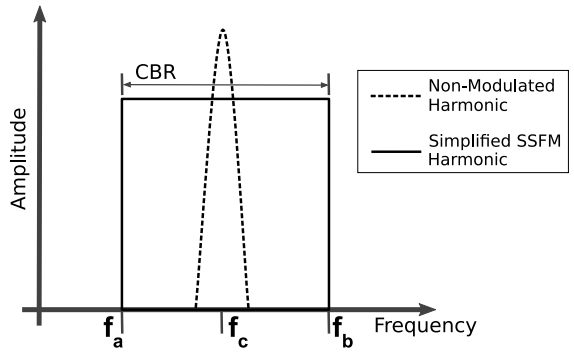

Fig. 3: A simplified representation of the effect of SSFM

where the $\text{SSFM}_{\text{peak}}$ is the height of the simplified SSFM harmonic.

As a comparison this estimation is applied to the values that are exhibited in Fig. 2. The resulting estimated peak value for the SSFM is 32.38 dBµV, a reduction from the non-modulated peak of 11.86 dBµV. The peak value of the SSFM modulated signal as simulated in Fig. 2 is 35.61 dBµV, a reduction of 8.63 dBµV.

The reason for the discrepancy is clear from Fig. 2; the spread spectrum is not flat topped but rather a collection of lesser peaks. Each empty space between these spread spectrum peaks means the reduction is less effective. Therefore, this indicates that greatest reduction in peak values can be found with the lowest f_m and the highest Δf_c, as this results in a 'flatter' and wider spectrum.

Indeed, this is the conclusion reached by previous works on the subject [4]–[6], [11], [12], [16].

C. Implementation Limitations

The chief limit imposed on SSFM parameters is the resolution bandwidth (RBW) used in the spectrum analyzer which measures the EMI. The RBW is the width of a band-pass filter applied to the incoming signal in a spectrum analyzer. During measurement, the center frequency of this filter is swept over the measurement frequency range. The power of the signal coming through the filter is recorded for each frequency point, which generates the frequency spectrum. A wider RBW decreases the measurement sweep time, however it results in a lower 'resolution' in the resulting spectrum.

If this resolution is too low, the effects of the SSFM are counteracted. Fig. 4 shows this effect as observed in a SPICE simulation of SSFM implementation. For this reason it is recommended in literature that $f_m \geq RBW$ [4], [5], [11].

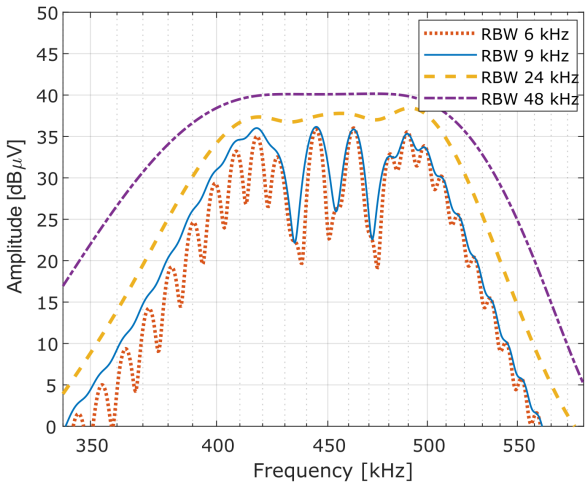

Fig. 4: The effect of RBW on average conducted EMI measurement from SPICE simulation of converter operating with $f_c = 455$ kHz, $f_m = 9$ kHz, $\Delta f_c = 60$ kHz

To ensure this is the case the f_m must be chosen accordingly as the RBW is determined by the EMC standard. In the case of the conducted emissions measurements at the switching frequency of 455 kHz (and up to 6.2 MHz) the RBW specified by CISPR-25 is 9 kHz [3]. CISPR-25 is used in this case as a relevant automotive standard.

The other easily manipulated parameter, Δf_c, does not have such a hard limit but is limited nonetheless due to the eventual overlap of the spectral components in higher harmonics.

As the harmonic number increases, the center frequency of that harmonic increases with $f_h = hf_c$. In conjunction, the bandwidth of each successive harmonic increases as well [5]:

$$B_h = 2(h\Delta f_c + f_m) \tag{6}$$

with h the harmonic number.

The overlap starts to occur when:

$$f_h + \frac{B_h}{2} = f_{h+1} - \frac{B_{h+1}}{2} \tag{7}$$

which can be solved for h and simplified when presuming that $f_c \gg f_m$:

$$h_{\text{overlap}} \approx \frac{2-\delta}{2\delta} \tag{8}$$

where $\delta = \frac{\Delta f_c}{f_c}$.

When overlap starts to occur, the peak reduction is less effective. Δf_c should be tuned to see the best

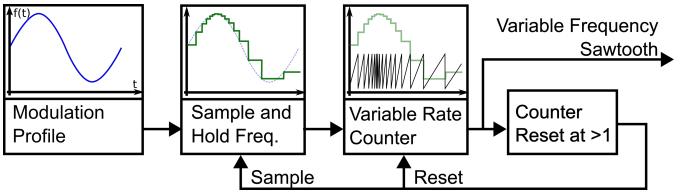

Fig. 5: Block Diagram of variable frequency sawtooth generation for use in variable frequency PWM generation

reductions in the regions where they are required to meet EMI standards. Another limit on Δf_c is the sizing of passives. These must be sized for the lowest switching frequency in the modulation.

III. SSFM In Simulation

This section will examine the specifics of implementing SSFM on the interleaved buck converter and the effects of different modulation profiles. A new modulation profile to fit the case of a converter with hardware filters is presented as well. SPICE simulations are used to evaluate the difference in EMI spectra of the variations discussed. The SPICE data is exported and processed in MATLAB to emulate the effect of the RBW in a spectrum analyzer.

A. Implemention of the Modulation in Simulation

One traditional scheme for creating a PWM waveform is to compare a duty-cycle input signal with a sawtooth waveform. The output of this greater-or-less-than comparison is a PWM waveform with a duty cycle equivalent to the input, and the frequency of the sawtooth wave. This sawtooth may be modulated with the desired SSFM parameters. This is accomplished with a system which is described by the diagram in Fig. 5.

Starting from the output, the variable sawtooth is generated by a counter that resets when it hits the upper threshold. This reset triggers a sampling of the modulated frequency reference signal, which sets the slope for the next counter cycle.

The question of appropriately phase shifting the SSFM switching across the phases of an interleaved converter is investigated by [6]. The conclusion of [6] for maximum EMI reduction when applied to two phases is to dynamically delay the second phase by half of each switching period. This variable delay switching frequency modulation (VDFM) has the downside of an increased low frequency (sub-harmonic) output ripple, but the best EMI peak reduction at switching frequency and above.

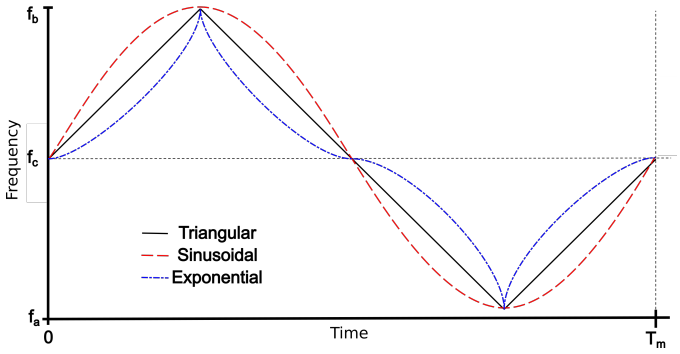

Fig. 6: Modulation profiles presented by previous works

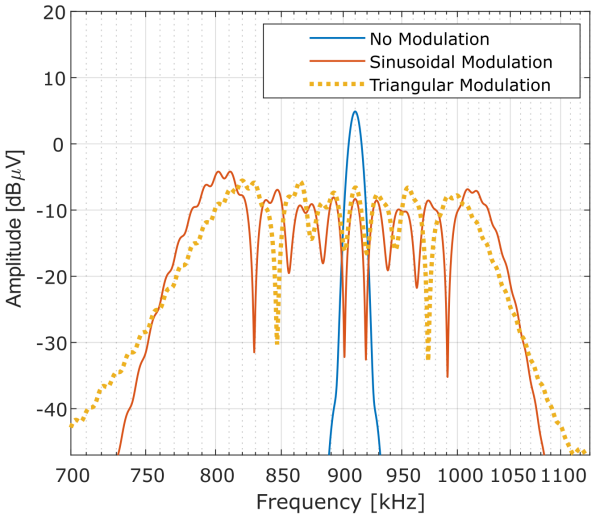

Fig. 7: Effect of modulation profiles on average conducted EMI from SPICE simulation, second harmonic. $f_{\mathrm{m}} = 9$ kHz, $\Delta f_{\mathrm{c}} = 60$ kHz for all modulations.

B. Modulation Profiles

Three main modulation profiles are investigated by previous works: sinusoidal, triangular, and exponential [5], [11], [12], [16]. These 3 modulation profiles are summarised in Fig. 6. While each of these works claims that a triangular modulation offers more reduction than a sinusoidal modulation, [16] claims that the exponential modulation is the best while the others find the opposite. The key differences between these works is the much higher frequencies used in [16] as well as the application in clocked digital circuits rather than PWM signals in power converters.

Only sinusoidal and triangular modulation are simulated here as the application here is more in line with the frequencies and context of [5], [11], [12]. The results are shown in Fig. 7.

In Fig. 7 the sinusoidal modulated spectrum has

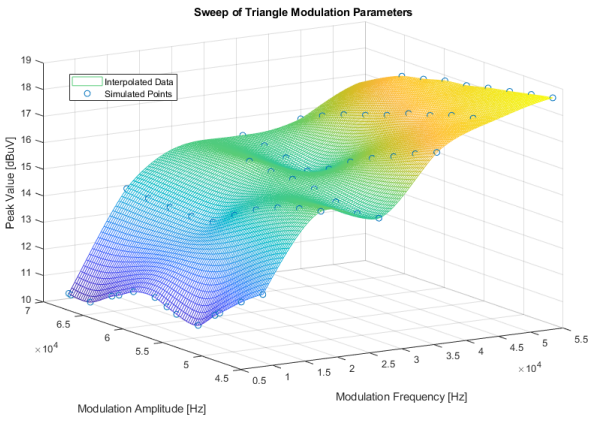

Fig. 8: A SPICE simulation sweep of f_m and Δf_c, and their effect on peak average conducted EMI values of the first harmonic for triangular SSFM, using an RBW of 9 kHz

higher peaks near the outer frequencies, but lower peaks in the center. This is due to the distribution over the frequency range of the sinusoidal modulation, where more switching happens at the frequencies near the edges of the modulation band. The triangular modulation on the other hand has a comparatively even top and thus a lower maximum peak. This effect of the modulation distribution will be exploited later.

C. Modulation Parameters

Using the simulations a sweep is performed of the f_m and Δf_c parameters in Fig 8. This is done using the triangular modulation profile, and confirms the general conclusions of previous works that a lower f_m and a higher Δf_c has lower peak values.

Some new observations, however, are that at lower values of f_m some local minima appear for the selection of Δf_c. These additional variations are rather small, at ≤ 1 dBµV between the local minima and adjacent local maxima, but so is the effect of Δf_c with $\leq$ 2 dBµV change over the swept range.

Compared to this, f_m has a greater effect in the lower values, but which tapers off when higher values for f_m are used.

D. Triangular Modulation Simulation Results

Shown in Fig. 9 is a view of the average conducted EMI spectrum from the interleaved converter as simulated in SPICE where the higher harmonics may be seen as well. For this simulation the converter is modelled including the filters as shown in 1, as these are also present on the hardware that will be tested later. The average conducted emissions are measured on the input side of the converter through a LISN also included in the model to match the later experimental testing setup.

The attenuation observed in this simulation is less than expected when compared to the previous literature [4]–[6], [11], [12], [16]. However, as will be seen later in section V-B the simulation used here also underestimates real world values by a significant margin. However, the relative effect of different modulations may still be evaluated through this simulation.

Despite this, a significant decrease in peak average conducted EMI values is observed. Crucially however, a significant slope is also observed along the top of the spread spectrum modulated harmonics. This is due to the LC filters (outlined in red in Fig. 1)) imposing a -40 dB/dec sloped attenuation on all frequencies above the cutoff frequency.

IV. SSFM for Filtered Applications

The previous literature referenced here on periodic SSFM use converters without filters for experimental verification. However, additional filtering may still be required for effects which are unmitigated by SSFM, or perhaps the required attenuation cannot be reached by SSFM alone.

The effect of additional hardware filtering can be taken advantage of in the modulation. As the hardware filters impart more attenuation on higher frequencies, the modulation can be biased to shift more energy into the region above center frequency.

A. Unbalanced Triangular Modulation

With a simple modification to the triangular modulation, the weight of the spread spectrum can be shifted. The unbalanced triangular profile in Fig. 10 is presented as a simple approach to obtain further peak reduction. Here, the amount of time spent switching above f_c in every modulation period is increased, thus putting more energy into the high side of the spectrum.

Compared to normal triangular modulation, using the unbalanced triangular profile with 55% of time spent above the center frequency 1.36 times more reduction on the first harmonic and 1.17 times on the third harmonic is achieved in SPICE simulation. The spectrum for this is shown in Fig. 11.

Yet as seen in Fig. 11, the unbalanced triangular spectrum does not make the spread spectrum harmonic peak flat-topped. Rather, the effect can be described as breaking up the sloped spread spectrum into two separate regions such that one may be offset without really counteracting the slope of the filter.

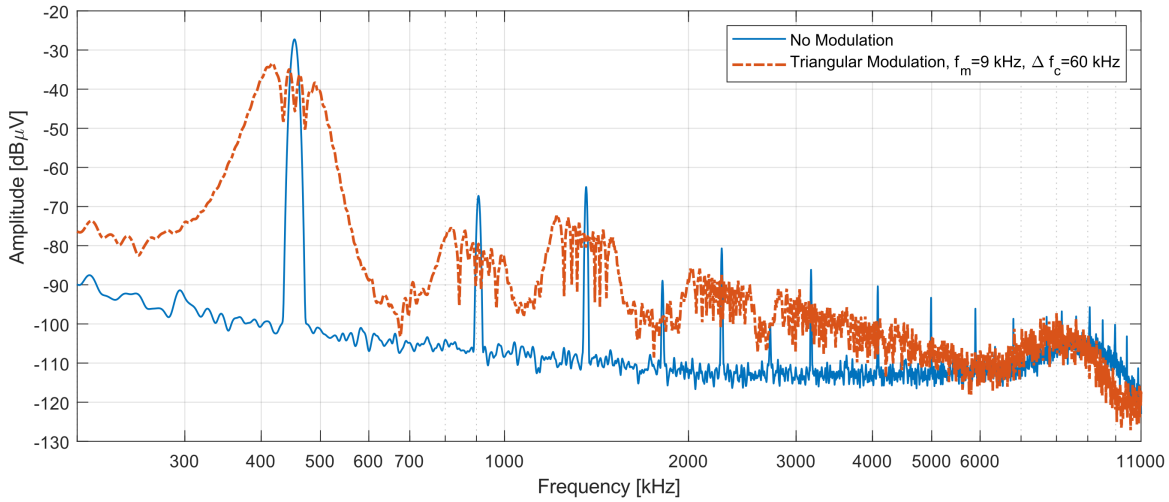

Fig. 9: Triangular SSFM average conducted emissions in SPICE simulation, input of interleaved buck converter with hardware LC filters.

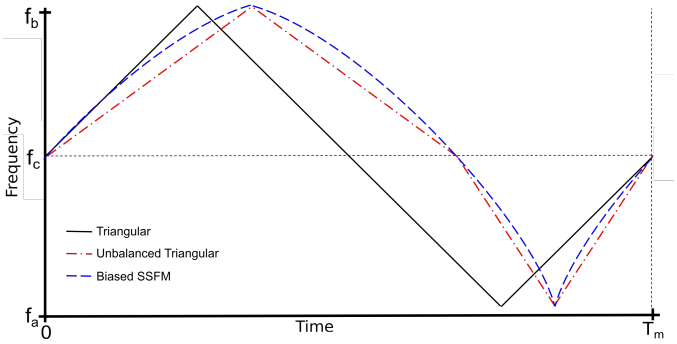

Fig. 10: Two new modulation profiles to shift the switching frequency balance towards the higher frequencies

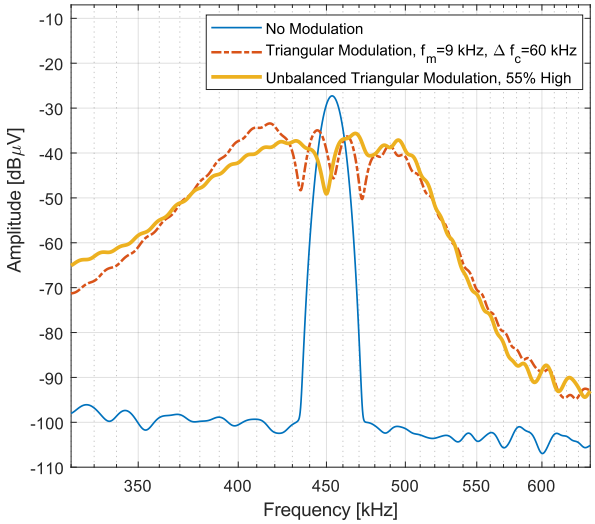

Fig. 11: Average conducted EMI of unbalanced triangular modulation and triangular modulation on input of interleaved buck converter as simulated in SPICE.

B. Biased Modulation

To better take advantage of the damping shape of the filters a biased modulation profile is developed. This modulation profile is generated by working backwards from the desired shape of the resulting EMI spectrum.

As was observed previously, the distribution of the modulating signal shapes the envelope of the resulting EMI spectrum. In other words, the envelope of the resulting EMI spectrum of these modulated signals is an imprint of the probability density function (PDF) of the modulating signal (in dB).

As the slope imparted on the spectrum by a first order LC filter is -40 dB/dec, the modulation generates a spectrum which has a +40 dB/dec slope (before filtering). Converting to the linear space, the modulating signal has a PDF describable by

$$y = Bx^2. \tag{9}$$

The selection of the coefficient B is based on the range of frequencies for that particular modulation. The integral of a PDF should be equal to 1, so

$$1 = \int_{f_a}^{f_b} Bx^2 dx. \tag{10}$$

From this, the coefficient B can be solved

$$B = \frac{3}{f_b^3 - f_a^3}, \tag{11}$$

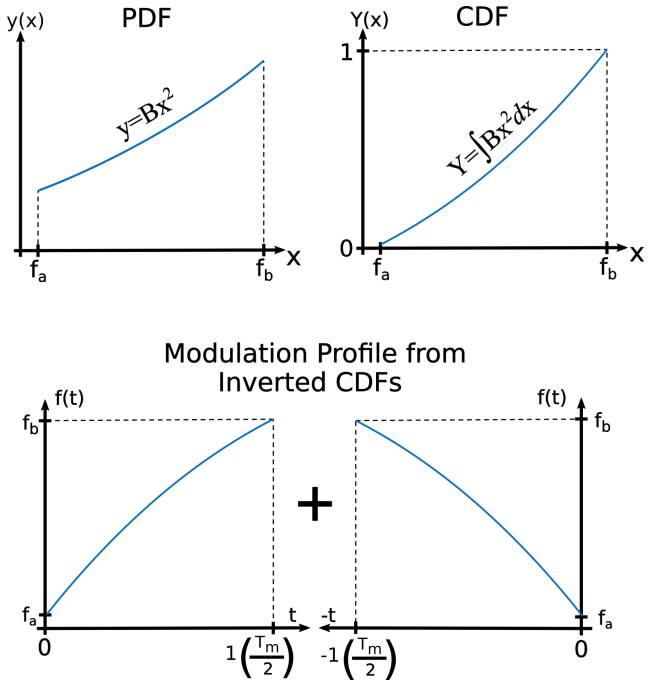

Fig. 12: Process for generating a modulation profile from a desired probability density function by inverting and scaling the CDF

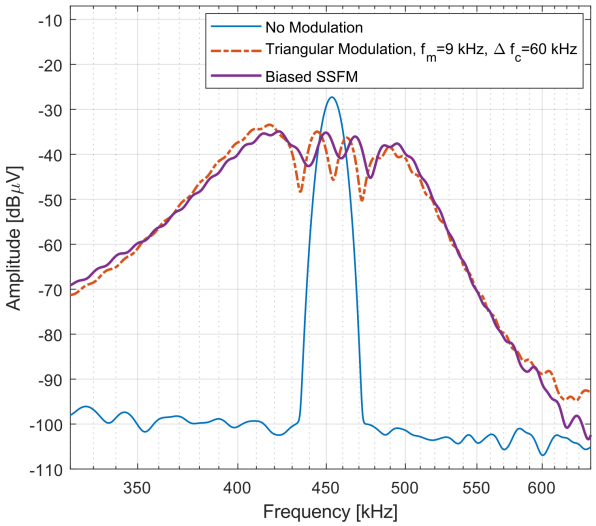

Fig. 13: Average conducted EMI of biased SSFM modulation and triangular modulation at the input of the interleaved buck converter as simulated in SPICE

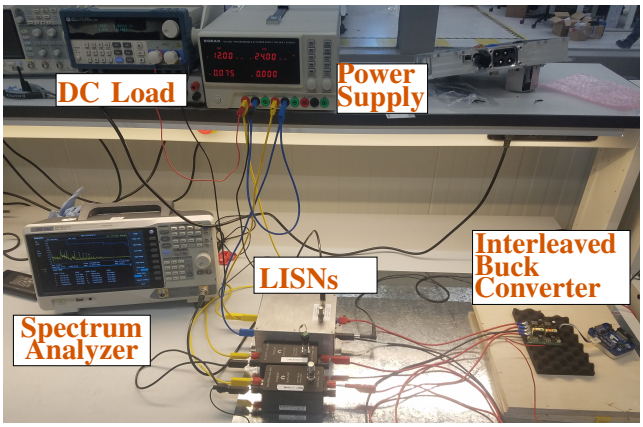

Fig. 14: EMI testing setup

where f_{min} and f_{max} are the limits of the desired modulation range. For a modulation with center $f_c = 455$ kHz and modulation amplitude $\Delta f_c = 60$ kHz an example PDF is shown in Fig. 12.

While a PDF is not unique to a particular function, it can be used to create a modulation profile. By integrating the PDF, the cumulative distribution function (CDF) is found, shown in Fig. 12. The CDF may be inverted and the new horizontal axis scaled to create a function in time with the same PDF/CDF.

In this case, the inverted CDF is combined with its reflection across the vertical axis to create a continuous and cyclical function, then scaled to match modulation frequency f_m. The resulting function in time is the "Biased SSFM" modulation profile shown in 10.

This profile is simulated in SPICE, and the peak reduction is similar to the unbalanced triangular modulation. However, as seen in Fig. 13 the slope along the top of the peaks is once again consistent as opposed to the unbalanced triangular modulation in Fig. 11.

V. Experimental Testing

A. EMI Testing Setup

Shown in Fig. 14 is the testing setup used for the average level conducted emissions testing on one of the inputs of the converter. This setup is as described in CISPR-25 [3], though with some differences. There is no shielded chamber, and thus the ground plane is also not bonded to the floor. The ground plane does not meet the minimum size specification, but is large enough to accommodate the device distance to edge specifications.

Some steps were taken to isolate the system from the grid connections, but due to equipment limitations some interfaces had to remain in place. While the microcontroller was powered by a battery, the main power loop still needed a bench power supply for the two 24 V inputs and an active DC load for the fixed 12 V output. Care was taken to place line impedance stabilization networks (LISNs) on each of these connections to isolate as much outside noise as possible, but as the later results will

show this was not entirely successful.

The spectrum analyzer parameters are within the limits described in CISPR-25 for these measurements. The spectrum analyzer is a Siglent SSA3021X Plus. The RBW is set at 9 kHz, the video bandwidth at 30 kHz, the step size at less than 5 kHz, and a little over 319 ms measurement time at each step.

An adjustment is also made to the implementation of the SSFM. Unlike what is shown in Fig. 5, the frequency of the switching is not updated on every PWM carrier reset. Due to the limitations of the microcontroller the switching frequency is updated on a 50 kHz interval.

B. Conducted EMI of SSFM

Shown in Fig. 15 are the average conducted emissions of the converter operating under triangular modulation and biased modulation both for 60 kHz and 100 kHz modulation amplitudes (with the non-modulated case for reference). Fig. 16 shows the peak conducted emissions spectra for the same. Tables I and II show the maximum magnitudes of the first harmonic for average and peak measurements, respectively. Due to range of the SSFM applied, the peak value of the first harmonic is taken in the range of frequencies from 355 kHz to 555 kHz.

TABLE I: Peak measured average EMI values of the first harmonic for various SSFM modulations

Modulation	**Max Value in First Harmonic [dBµV]**	**Reduction in Max [dBµV]**
No Modulation	56.18	-
Triangular Modulation $\Delta f_c = 60$ kHz	45.05	11.13
Triangular Modulation $\Delta f_c = 100$ kHz	42.35	13.83
Biased Modulation $\Delta f_c = 60$ kHz	45.30	10.88
Biased Modulation $\Delta f_c = 100$ kHz	43.25	12.94

As seen in Tables I and II, the reduction of the maximum values is rather similar for each modulation. The biased modulations even consistently perform worse than the triangular modulation of the same amplitude.

Despite this, examining the first through fifth harmonics in Figs. 15 and 16 shows that the biasing effectively modifies the slope along the top of the spread harmonic spectra. However, the slope along these tops of the triangular modulations is not as steep as was expected based on simulation of the converter. Hence, the biased modulation is over correcting.

Looking to the higher order harmonics, as the overlap between the harmonics starts to occur the shaping due to the modulation profile disappears. In average detector measurements, Fig. 15, there is no more reduction around 10 MHz with the 'noise floor' raised to where the peaks were previously present. Yet in peak detection, Fig. 16, the reduction in the spectrum continues with sustained effectiveness into this region.

TABLE II: Peak measured peak EMI values of the first harmonic for various SSFM modulations

Modulation	**Max Value in First Harmonic [dBµV]**	**Reduction in Max [dBµV]**
No Modulation	56.84	-
Triangular Modulation $\Delta f_c = 60$ kHz	50.60	6.24
Triangular Modulation $\Delta f_c = 100$ kHz	47.99	8.84
Biased Modulation $\Delta f_c = 60$ kHz	51.02	5.81
Biased Modulation $\Delta f_c = 100$ kHz	48.91	7.93

C. Efficiency Testing Setup

For testing the efficiency the setup is similar to the EMI testing, but without the LISNs. A PPA5500 3-channel power analyzer with internal shunts and remote voltage sensing is used to measure the voltage and current of the two input phases and single output of the converter.

The gate driving circuitry is powered on-board and so these losses are taken into account. However, the micro controller is again powered separately. Any additional power consumed in processing is therefore not included in the following results. As the constant application of a new switching frequency is required to successfully carry out the modulation, some more processing capability (or more specialized hardware such as an FPGA) is required.

It was noted during testing that depending on the code implementation and compiler settings, the power consumption of the micro controller could increase to a point which is significant at these power levels. The micro controller power consumption was not included in the efficiency results.

D. The effect of SSFM on Efficiency

Shown in Fig. 18a is a collection of efficiencies of operation with unbalanced triangular modulations which are progressively more biased towards higher frequency switching. With this converter, spending more time switching at the frequencies above 455 kHz appears to have little effect on efficiency. It should also be noted that the unbalanced triangular modulation with 62% of

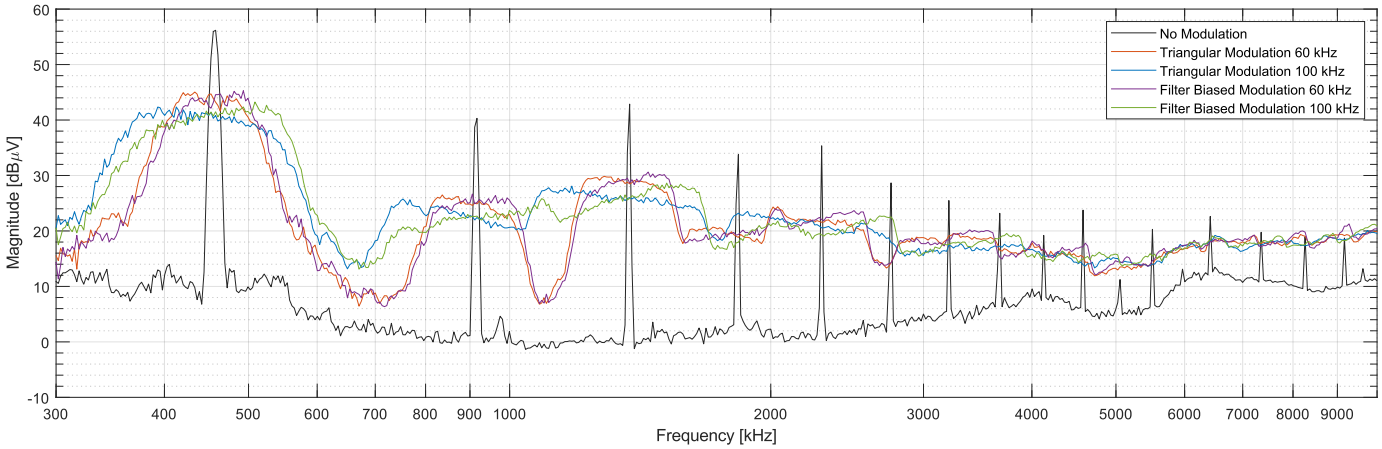

Fig. 15: Average detector conducted emissions measured on one converter input, from 300 kHz to 10 MHz

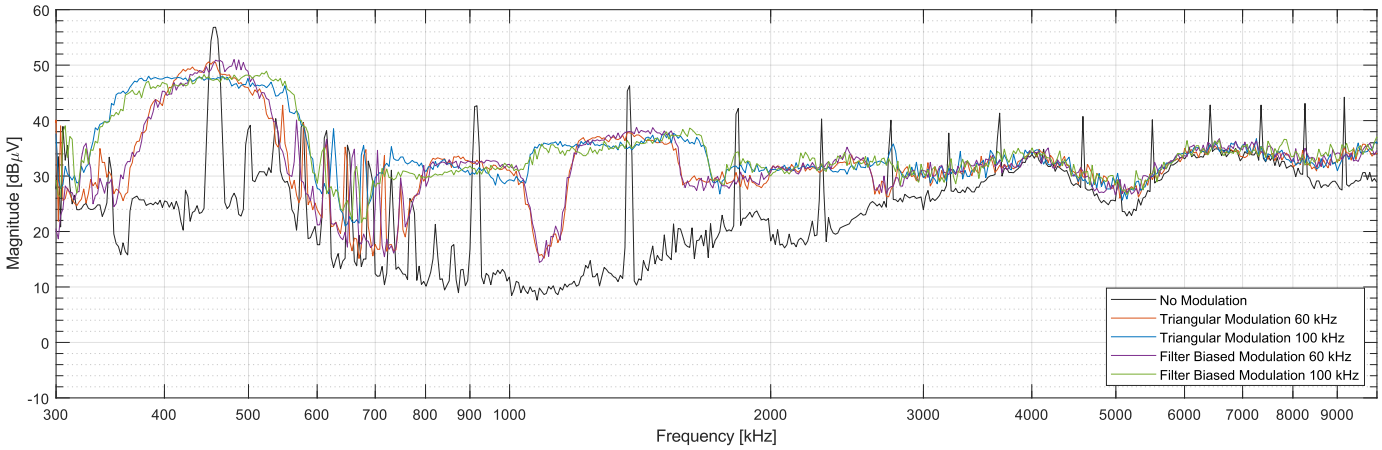

Fig. 16: Peak detector conducted emissions measured on one converter input, from 300 kHz to 10 MHz

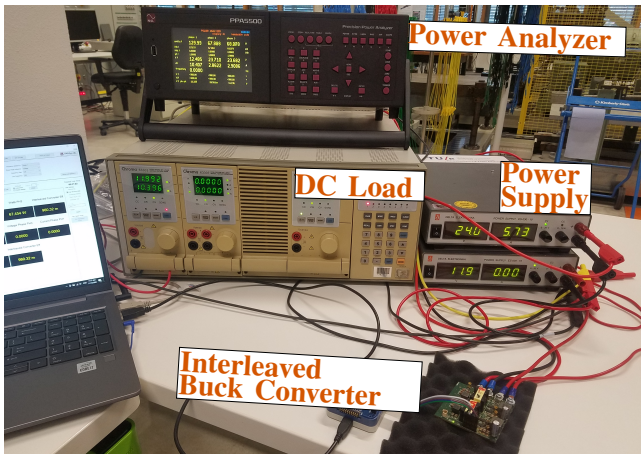

Fig. 17: Efficiency testing setup

the switching time above 455 kHz is the closest match to the biased SSFM modulation profile. The 75% unbalanced triangular modulation is included to investigate the extremes of the useful application of this technique.

Next, Fig 18b shows two different modulations with a similar distribution of frequencies but for different modulation amplitudes. Here there is again no clear difference in efficiency.

Finally, Fig. 18c shows this selection of modulations against the non-modulated case. Here there is an observable difference to the operational efficiency of the converter at lower powers, up to and including the peak efficiency point at around 51 W output power. When any SSFM profile is used, around 0.059% of efficiency is lost from the peak efficiency, which is around 29.5 mW of additional losses in this converter. A larger output voltage (and current) ripple is present with these modulations.

At higher power levels there is no longer a clear difference in efficiency between the modulated and non-modulated modes of operation, the ripple does not increase with load.

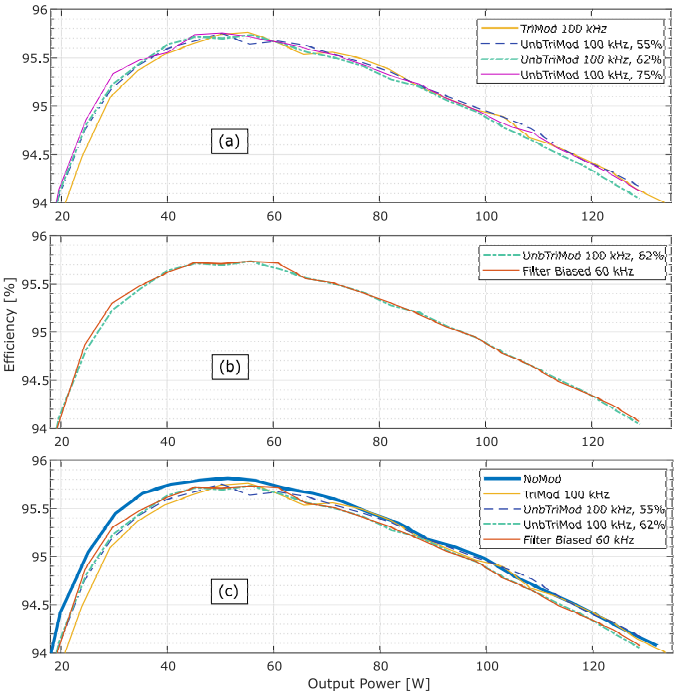

Fig. 18: Converter efficiency for (a) higher frequency biased modulations, (b) higher amplitude modulations, and, (c) compared to the non-modulated case.

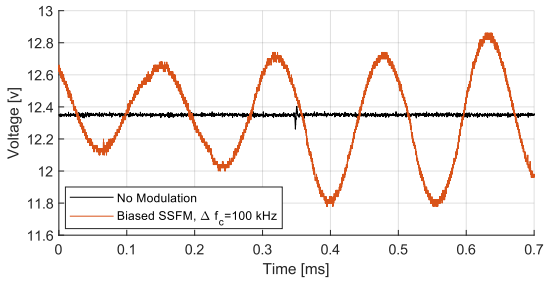

Fig. 19: Voltage ripple measured on the interleaved buck converter output

E. Output Voltage Ripple

As reported in [6], an increased sub-harmonic output voltage (and current) ripple is observed when the VDFM SSFM used here is applied. However, while the ripple reported in [6] is 23.3 mV_{pp}, the ripple in the converter used here is orders of magnitude larger as shown in Fig. 19. Ranging between 0.5 V_{pp} to 1 V_{pp} the ripple is not consistent over time, but is observed regardless of the variation of the modulation used.

With VDFM each phase's switching frequency is updated on its own PWM carriers' reset. Hence, in a 2-phase interleaved converter the second phase always updates half a switching period later than the first. This causes an imbalance in the volt-second balance of each phase. Unlike the true VDFM implementation simulated in Section III, the adjusted version implemented in Section V-A allows more switching cycles for this imbalance to bias the output currents as the volt-second balance recovers. This phase-to-phase dynamic has very little damping so quickly the output ripple becomes quite large.

In this 2-phase converter a triangular PWM carrier with double update can be used to update switching frequency in both phases simultaneously without creating this imbalance hence the adjusted VDFM can be used, but this solution cannot be extended to arbitrary interleaved phases. Alternately, it is shown by [17] that this ripple can be drastically reduced in control though this is with true VDFM.

VI. Conclusion

The theory of SSFM and a simplified analytical analysis is presented. The limitations of the technique as presented by previous works are explored. Some simulations of the technique are carried out to verify the applicability of the referenced literature conclusions when applied to the two phase interleaved buck converter examined in this paper.

The shortcomings of previously presented modulation schemes in regards to a converter with hardware filters are observed, and some new modulation profiles are presented to deal with these limitations. Though these modulation profiles work to shape the spectrum well in simulation, there is an over correction in hardware testing.

Finally, hardware tests of these techniques reveal some trade-offs in other areas of converter performance. Some effect on efficiency is noticeable in lower power levels but are of lesser consequence in higher powers. Some increased computation requirements are present. A pronounced output voltage ripple can be observed, yet can be dealt with in a variety of ways.

Despite these limitations, SSFM is an effective tool to reduce conducted EMI around the switching harmonics. The biasing in the modulation profiles can be used to shape the spectrum where necessary.

References

[1] C. R. Sullivan and M. J. Powers, "A high-efficiency maximum power point tracker for photovoltaic arrays in a solar-powered race vehicle," 1993.

[2] H.-P. Park, H.-J. Choi, and J.-H. Jung, "Design and implementation of high switching frequency llc resonant converter for high power density," in *2015 9th International Conference on Power Electronics and ECCE Asia (ICPE-ECCE Asia)*, 2015, pp. 502–507.

[3] *Vehicles, boats and internal combustion engines - Radio disturbance characteristics - Limits and methods of measurement for the protection of on-board receivers*, CISPR-25, 2016.

[4] J. Balcells, A. Santolaria, A. Orlandi, S. Member, D. González, and J. Gago, "Emi reduction in switched power converters using frequency modulation techniques," *IEEE TRANSACTIONS ON ELECTROMAGNETIC COMPATIBILITY*, vol. 47, p. 569, 2005.

[5] A. Santolaria, J. Balcells, and D. Gonzalez, "Theoretical and experimental results of power converter frequency modulation," 2002.

[6] J. Mon, D. González, J. Balcells, J. Gago, and P. Bogónez, *Hybrid Modulator for power converters in parallel topology*, 2012.

[7] M. M. Bech and J. K. Pedersen, "Random modulation techniques with fixed switching frequency for three-phase power converters," p. 753, 2000.

[8] G. M. Dousoky, S. Member, M. Shoyama, S. Member, and T. Ninomiya, "Fpga-based spread-spectrum schemes for conducted-noise mitigation in dc-dc power converters: Design, implementation, and experimental investigation," *IEEE Transactions on Industrial Electronics*, vol. 58, p. 429, 2011.

[9] H. Li, Y. Liu, J. Lü, and X. Yu, "Suppressing emi in power converters via chaotic spwm control based on spectrum analysis approach," *IEEE TRANSACTIONS ON INDUSTRIAL ELECTRONICS*, vol. 61, 2014.

[10] K. K. Tse, R. W.-M. Ng, H. S.-H. Chung, and S. Y. R. Hui, "An evaluation of the spectral characteristics of switching converters with chaotic carrier-frequency modulation; an evaluation of the spectral characteristics of switching converters with chaotic carrier-frequency modulation," *IEEE Transactions on Industrial Electronics*, vol. 50, 2003.

[11] D. González, J. Balcells, A. Santolaria, J.-C. L. Bunetel, J. Gago, D. Magnon, and S. Bréhaut, "Conducted emi reduction in power converters by means of periodic switching frequency modulation," *IEEE TRANSACTIONS ON POWER ELECTRONICS*, vol. 22, 2007.

[12] A. Santolaria, J. Balcells, D. Gonzalez, and J. Gago, "Evaluation of switching frequency modulation in em1 emissions reduction applied to power converters," 2003.

[13] S. U. Hasan and G. E. Town, "An aperiodic modulation method to mitigate electromagnetic interference in impedance source dc-dc converters," *IEEE Transactions on Power Electronics*, vol. 33, pp. 7601–7608, 9 2018.

[14] S. Johnson and R. Zane, "Custom spectral shaping for emi reduction in high-frequency inverters and ballasts," *IEEE TRANSACTIONS ON POWER ELECTRONICS*, vol. 20, p. 1499, 2005.

[15] R. C. Dixon, *Spread Spectrum Systems*. J. Wiley, 1984.

[16] K. B. Hardin, J. T. Fessler, and D. R. Bush, "Spread spectrum clock generation for the reduction of radiated emissions," 1994.

[17] D. González, J. T. Bialasiewicz, J. Balcells, and J. Gago, "Wavelet-based performance evaluation of power converters operating with modulated switching frequency," *IEEE Transactions on Industrial Electronics*, vol. 55, pp. 3167–3176, 2008.